Control and Simulation of a Current-Fed Linear Inductor Machine

BIMAL K. BOSE, SENIOR MEMBER, IEEE, AND THOMAS A. LIPO, SENIOR MEMBER, IEEE

Abstract—**A self-controlled, current-fed inverter excited linear inductor machine is described, in which the field current and inverter switching angles are programmed such that the machine operates at constant air-gap flux and unity displacement factor under all operating conditions. The machine can operate in wide speed range and constant predetermined torque is developed during both motoring and regeneration. The control incorporates overlap angle compensation for the inverter and permits modulation of inverter firing angle with resolution of a fraction of a degree. The dynamic *d-q* axis model of the machine with the power converters and the proposed control strategy has been simulated on a hybrid computer, and static and dynamic performance have been studied in detail. The control circuit has been designed and tested with a 112-kW prototype inductor machine. The experimental results give good agreement with the theory and with simulation.**

I. INTRODUCTION

THE CURRENT-SOURCE inverter fed synchronous machine drives with a self-control feature (also known as commutatorless machine) have attracted increasing interest in recent years [1]. In this class of drives, the power conversion circuit is simple for bidirectional power control, and load commutation can be implemented if the machine is permitted to operate at a certain minimum leading displacement factor. The self-controlled synchronous machine behaves as a "modified" dc machine which can be operated in wide speed and torque ranges with very little stability problems and with no fear of pulling out of step. An inductor-type machine has the added advantage of higher speed capability because the rotor dc field is excited from the stator side. Therefore, the machine is attractive for applications such as flywheel energy storage, aircraft generators, linear motor propulsion, and other high-speed applications.

In this paper a speed control system is described for a homopolar, sector wound inductor machine [2]. This sector-type machine is, in fact, a laboratory model of linear synchronous motor propulsion system which is presently under test in a high speed rail propulsion program sponsored by the U.S. Department of Transportation. In the present control strategy the field current and inverter firing angles are regulated such that the machine always operates at constant air-gap flux and the terminal displacement angle is zero under all operating conditions. Maintaining constant rated air-gap flux allows optimum utilization of the magnetics, and unity displacement factor permits efficient and economical design of the inverter and machine as a system [3].

Paper ID 78-1, approved by the Industrial Drives Committee of the IEEE Industry Applications Society for presentation at the 1978 Industry Applications Society Annual Meeting, Toronto, ON, Canada, October 1–5. Manuscript released for publication November 8, 1978.

B. K. Bose is with the Corporate Research and Development Center, General Electric Company, Schenectady, NY 12301.

T. A. Lipo was with General Electric Company, Schenectady, NY. He is now with Purdue University, Lafayette, IN.

II. DESCRIPTION OF CONTROL SYSTEM

Fig. 1 shows the power circuit of the drive system and Fig. 2 gives the idealized voltage and current waves at the machine terminal for unity displacement factor. Three-phase 60-Hz ac power at the input is converted to dc by a phase-controlled bridge rectifier, and is then inverted by an auto-sequential type force-commutated inverter to generate three-phase variable-frequency variable-current power for the inductor machine. Ignoring the forced commutation circuit of the inverter, both sides of the power circuit are symmetrical about the dc link. Since the machine displacement factor is constrained to be unity during both motoring and regeneration, the inverter firing angle with respect to machine phase voltage is 0° during motoring mode but switches to 180° during regeneration.

The general control block diagram of the system is shown in Fig. 3. It can be noted that the machine has two main feedback control loops, a speed control in the outer loop and a torque control in the inner loop. The command speed ω^* in the system is compared with the feedback speed ω_r, and the resulting error signal generates the armature current command I_a^* of the machine. Under the condition of constant air-gap flux and unity terminal displacement factor, it can be shown that the developed torque of the machine is proportional to armature current amplitude I_a. Since the rectifier input current amplitude I_a' has essentially the same amplitude as I_a it has been used as feedback signal because it is derived from currents having a constant 60-Hz frequency. The absolute value circuit maintains a positive polarity for the commanded value of armature current I_a^*, which is symmetrical with minimum and peak values clamped during both motoring and regeneration.

The I_a^* signal is used to generate the field current command I_f^* and the armature current phase angle command ϕ^* through the respective function generator as shown in the figure. The polarity of ϕ^* signal depends on the polarity of speed error which in turn governs the motoring or regeneration mode. The derived phase angle is then subtracted from the bias angle of 180° to generate the switching delay angle α_d. The self-control circuit of the machine consists of a set of position sensors, digital angle controller, and the thyristor firing circuit which will be described later.

Overlap Angle Compensation

The actual phase current wave of the machine deviates from the ideal six-step wave due to commutation effect as shown in

0093-9994/79/1100-0591$00.75

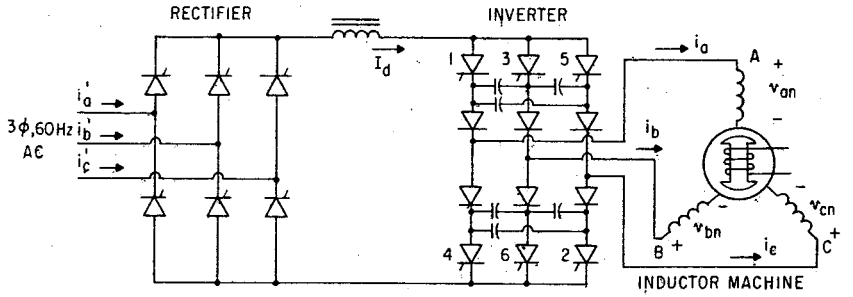

Fig. 1. Power circuit of the drive system.

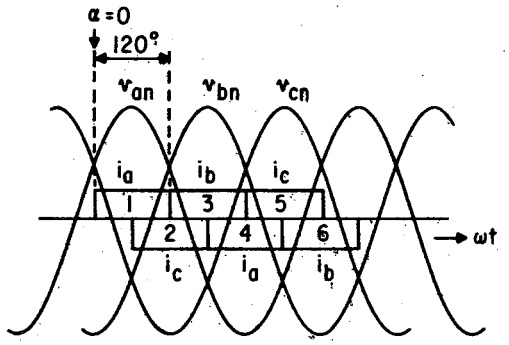

Fig. 2. Idealized voltage and current waves at unity.

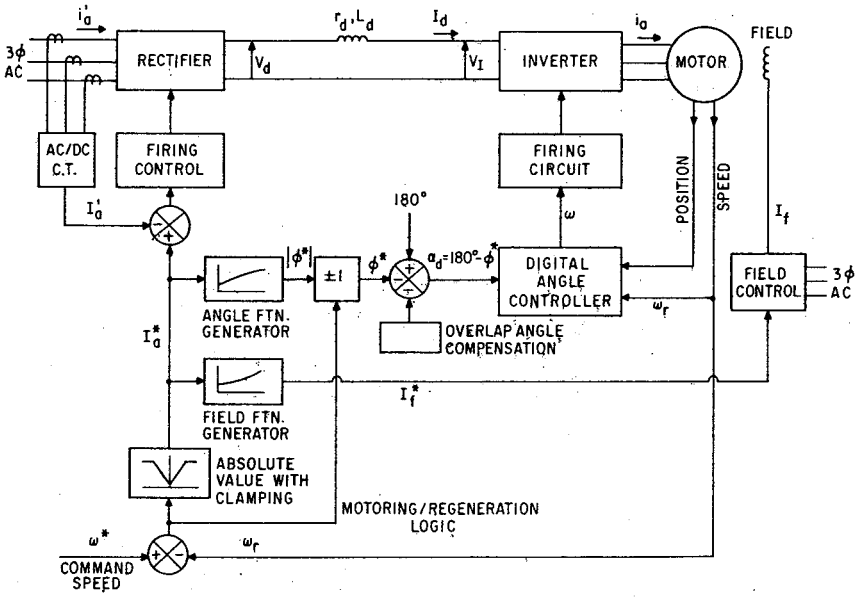

Fig. 3. General control block diagram.

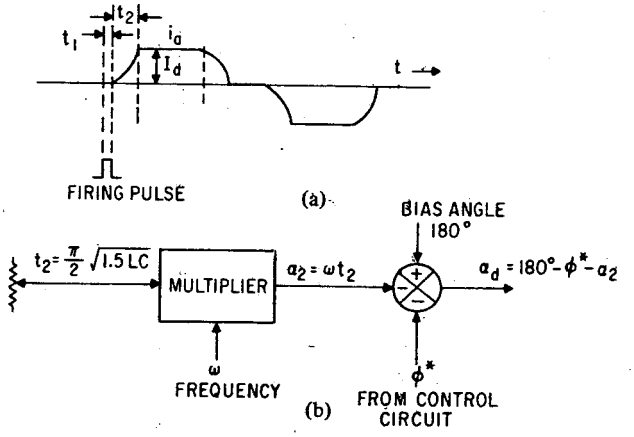

Fig. 4. Overlap angle compensation.

Fig. 4(a). From the instant of firing the SCR, the phase current rises to maximum value I_d after a delay $t_1 + t_2$, where t_1 = constant current charging time of commutation capacitors and t_2 = delay corresponding to overlap angle α_2. In the practical operating range, t_1 can be neglected and $t_2 = \pi/2\sqrt{1.5LC}$, where L and C are commutating inductance and capacitance, respectively. Since L and C are constant parameters, the phase angle delay due to commutation can be compensated by the circuit as shown in Fig. 4(b). The signal t_2 is multiplied by angular frequency ω to construct α_2 which is then subtracted from α_d to give the equivalent phase lead of inverter switching angles.

III. DERIVATION OF ϕ^* AND I_f^* SIGNALS

Fig. 5 shows the phasor diagrams of the machine for both motoring and regeneration at unity displacement angle, and Fig. 5 shows the corresponding waveforms. The stator resistance has been neglected for simplicity.

Relating to the phasor diagram for motoring, the following expressions can be written in standard symbols:

$$X_{ds} = \omega_b L_{ds} \tag{1}$$

$$X_{qs} = \omega_b L_{qs} \tag{2}$$

$$X_{ad} = \omega_b L_{ad} \tag{3}$$

$$\psi_{ds} = X_{ds} I_{ds} = X_{ds} I_a \sin \delta \tag{4}$$

$$\psi_{qs} = X_{qs} I_{qs} = X_{qs} I_a \cos \delta \tag{5}$$

$$\psi_f = X_{ad} I_f' \tag{6}$$

$$I_f = \frac{I_f'}{N} \tag{7}$$

$$E_a = \frac{\omega}{\omega_b} E_A = \frac{\omega}{\omega_b} \psi_f \tag{8}$$

$$V_t = \frac{\omega}{\omega_b} V_T = \frac{\omega}{\omega_b} \psi_t \tag{9}$$

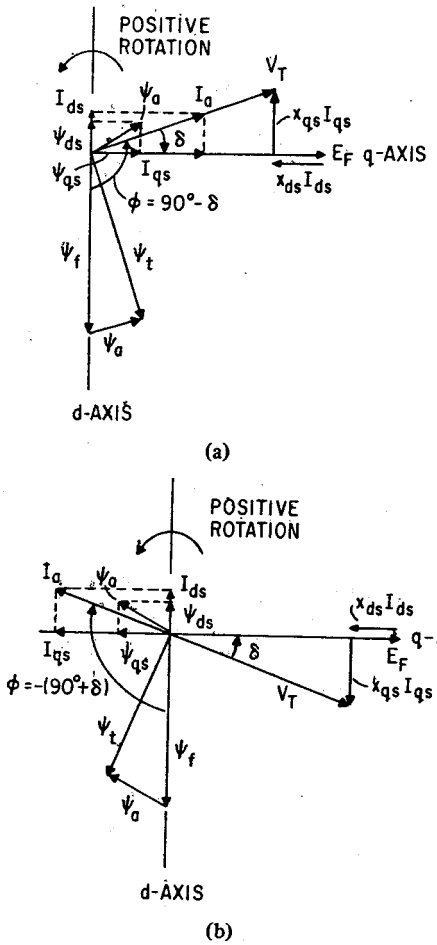

Fig. 5. Phasor diagram. (a) Motoring mode. (b) Regeneration mode.

$$\phi = 90° + \delta \tag{10}$$

$$\bar{\psi}_t = \bar{\psi}_f + \bar{\psi}_a \tag{11}$$

$$\tan \delta = \frac{X_{qs} I_{qs}}{E_f - X_{ds} I_{ds}}. \tag{12}$$

In (1)-(12), ω_b is a constant base or design frequency used to define the machine reactances, and ω is the operating frequency. The voltage V_t is the machine terminal volts at operating angular frequency ω, whereas V_T is the terminal voltage at base frequency. Similarly, E_a and E_A are the Thevenin internal EMF's at ω and ω_b, respectively.

From (11),

$$\psi_t^2 = (\psi_f - \psi_{ds})^2 + \psi_{qs}^2. \tag{13}$$

Combining (13) with (1)-(6) and (9),

$$V_T^2 = (X_{ad} I_f' - X_{ds} I_a \sin \delta)^2 + X_{qs}^2 I_a^2 \cos^2 \delta. \tag{14}$$

Combining (3), (6), (8), and (12)

$$\tan \delta = \frac{X_{qs} I_{qs}}{X_{ad} I_f' - X_{ds} I_{ds}}. \tag{15}$$

Substituting (4) and (5) in (15) and simplifying

$$\left(\frac{X_{ds}}{X_{qs}}-1\right)\sin^2\delta-\frac{X_{ad}}{X_{qs}}\frac{I_f'}{I_a}\sin\delta+1=0. \tag{16}$$

Equations (14) and (16), respectively, can be written in normalized form as follows:

$$\left(\frac{I_f'}{I_a}-\frac{X_{ds}}{X_{ad}}\sin\delta\right)^2+\frac{X_{qs}^2}{X_{ad}^2}(1-\sin^2\delta)=\frac{V_T^2}{X_{ad}^2I_a^2} \tag{17}$$

and

$$\frac{I_f'}{I_a}=\frac{1+\left(\frac{X_{ds}}{X_{qs}}-1\right)\sin^2\delta}{\frac{X_{ad}}{X_{qs}}\sin\delta}. \tag{18}$$

Equations (7), (10), (17), and (18) can be solved numerically with the given machine parameters in Table I to express ϕ^* and I_f^* as function of I_a^*.

IV. ROTOR POSITION SENSING PRINCIPLE

An optical interruption method of position sensing is used in the present system as illustrated in Fig. 6. There are six stationary optical sensors which generate parallel and independent firing pulses for each of the inverter SCR's. Each sensor consisting of a light emitting diode, phototransistor and pulse amplifying circuit is positioned at 60 electrical degrees interval on one side of the rotor drum. A round interrupting stud is mounted on the rotor at the center line of each north pole. As the machine rotates in the direction shown, the rotor position encoded pulses are generated in the sequence 1-2-3-4-5-6 which are then fed at the input of the digital angle controller circuit.

V. DIGITAL ANGLE CONTROLLER

The function of the angle controller is to delay the set of position encoded pulses proportional to the analog signal α_d which then generate the corresponding firing pulses of the inverter SCR's. This digital control method has the advantage that it eliminates offset and drift errors and prevents any asymmetry in SCR firing.

Since the ideal machine phase current flows in 120° pulses, the SCR for the corresponding phase is switched on 60° earlier to satisfy the fundamental frequency wave relations as shown in Fig. 7. The rotor position encoded pulse for a particular phase polarity is generated with a 240° lead angle with respect to positive peak value of ψ_f wave so that the SCR switching delay angle is given by $\alpha_d = 180° - \phi$ where ϕ is positive for motoring and negative for regeneration. In the present design, $\phi_{max} = 128°$ (corresponding to $\delta_{max} = 38°$) which keeps a margin of 52° for overlap angle compensation.

A schematic of the angle controller is shown in Fig. 8 and its operation is explained in Fig. 9. There are six identical parallel channels each of which receives position encoded

TABLE I
PARAMETERS OF THE SIMULATED MACHINE

	Simulated	Constructed
Power	112 kW	77 kW
Armature Current	281 Amps	370 Amps
Phase Voltage	140 Volts	87 Volts
Wheel Speed	1526 RPM (111 m/s)	1526 RPM
Frequency	394 Hz (ω_b= 2476 rad/s)	394 Hz
Rotor Poles	30	30
Stator Poles	3.5 (Effective)	5.0
δ_{max}	38°	38°
Stator Resistance r_s	0.0258 Ω	0.013 Ω
Stator Leakage Reactance $X_{\ell s}$	0.208 Ω	0.14 Ω
d-Axis Stator Magnetizing Reactance X_{ad}	0.25 Ω	0.17 Ω
q-Axis Stator Magnetizing Reactance X_{aq}	0.222 Ω	0.14 Ω
d-Axis Stator Self-Reactance $X_{ds} = X_{\ell s} + X_{ad}$	0.458 Ω	0.31 Ω
q-Axis Stator Self-Reactance $X_{qs} = X_{\ell s} + X_{aq}$	0.43 Ω	0.28 Ω
Field Leakage Reactance $X'_{\ell f}$ (Referred to Stator)	0.2371 Ω	0.47 Ω
Field Resistance r'_f (Referred to Stator)	0.229 Ω	0.2125 Ω
Field/Stator Effective Turns Ratio N	4.06	9.0

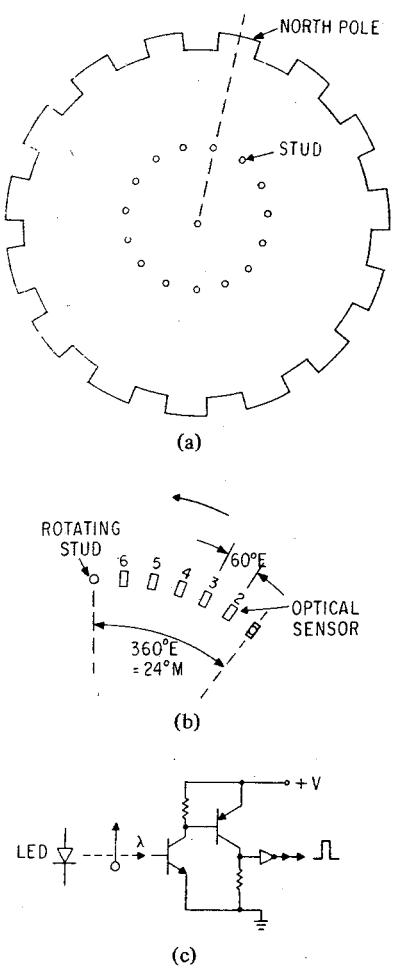

Fig. 6. (a) Rotor end view showing light interrupting studs. (b) Optical sensor configuration. (c) Sensor circuit.

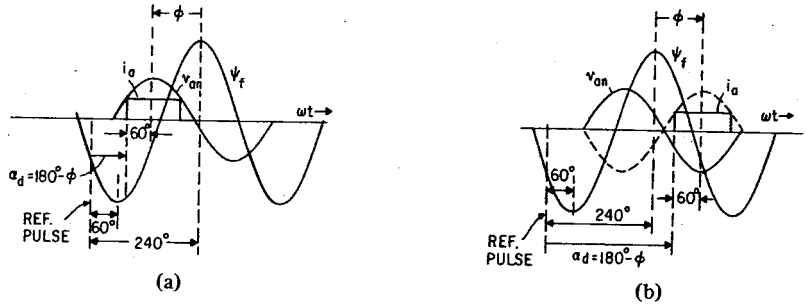

Fig. 7. Idealized waveforms. (a) Motoring mode. (b) Regeneration mode.

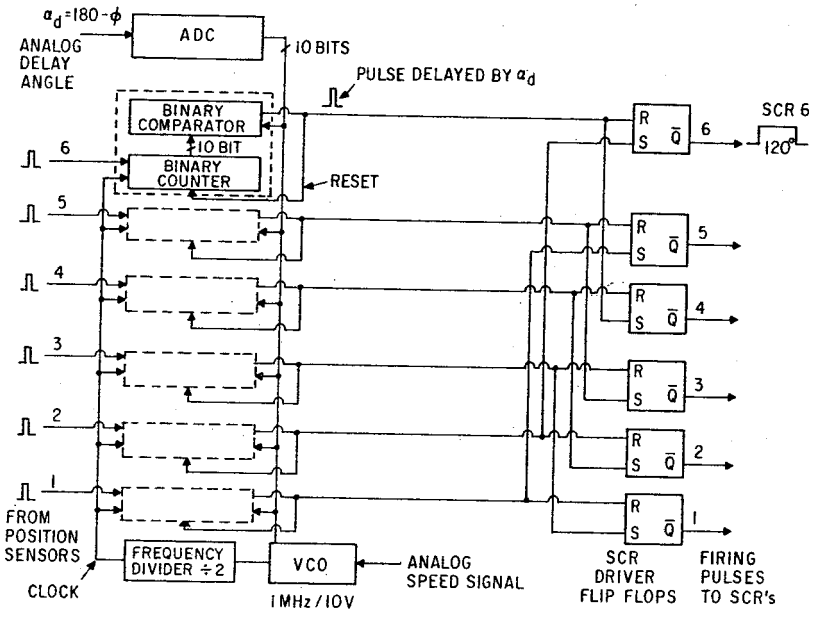

Fig. 8. Schematic of angle controller.

pulses at the input and generates the firing pulse for the corresponding SCR at delay angle α_d. The circuit uses the digital ramp comparison principle and generates the time delay $t_d = \alpha_d/\omega$, where ω is the inverter angular frequency. The ADC box converts the analog signal into the equivalent digital word. A clock proportional to the inverter frequency is generated from the speed signal and fed to the binary counter. The position encoded pulse 'enables' the counter to ramp up with a slope proportional to ω as shown in Fig. 9. The binary comparator compares the counter and ADC outputs and generates a pulse at the crossover point which corresponds to the delay angle α_d. If α_d is fixed, but speed is reduced, the time delay extends proportionately to maintain same α_d. The comparator output also resets the counter which is enabled again after time period $T = 2\pi/\omega$. The output pulses in parallel are combined in driver flip-flops to generate 120° wide firing pulses.

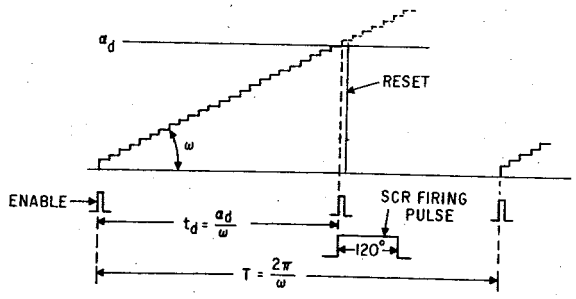

Fig. 9. Operation of angle control circuit.

VI. HYBRID COMPUTER SIMULATION

In order to gain insight into the effectiveness of the control scheme the entire system including current source inverter, filter, inductor machine, and associated control system was simulated on the hybrid computer. Such an analysis phase is extremely useful in the design of any converter system since it makes available a "breadboard" for the adjustment of those regulator gains, time constants, and maximum and minimum limits [4] which can best be accomplished by experimentation. Since this phase can be completed well in advance of construction, modifications to the control can be easily incorporated without delays in the assembly of the hardware. The system can also be exercised over all modes of operation and a high degree of confidence established before the design is put to hardware.

Fig. 10 shows the basic simulation that was used to model the four-pole inductor-type synchronous machine. The actual machine is a sector-type motor rated at 150 hp (112 kW). Details of the machine parameters are given in Table I. Since

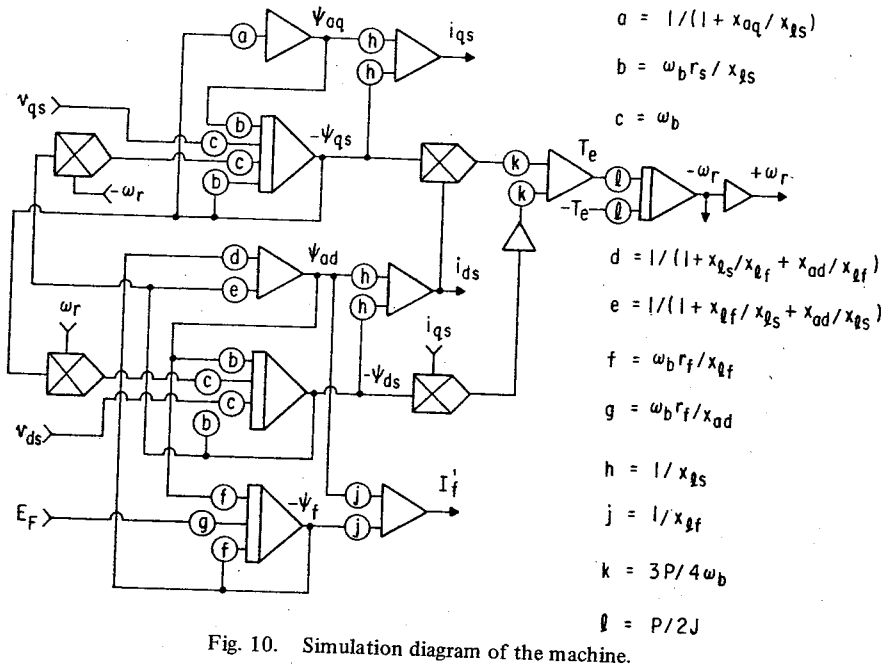

Fig. 10. Simulation diagram of the machine.

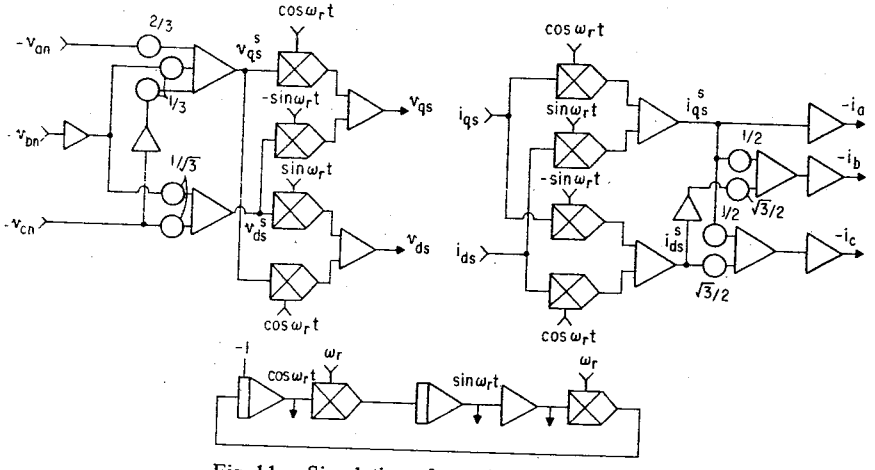

Fig. 11. Simulation of transformation equations.

the machine is essentially a linear motor with a finite length the equations describing its operating behavior are not well documented. However, a detailed analysis of this machine has indicated that the static entry and exit effects can be considered as negligible [5]. Hence the machine operates essentially as an ideal cylindrical four-pole inductor machine which can be modeled adequately by Park's equations [6], [7]. Also, the rotor saliencies are constructed of finely laminated steel without damper windings. Hence the eddy currents in the rotor resulting from rotation (dynamic end effects) can be ignored. Correspondingly, simulation of the machine need not contain extra rotor circuits to account for amortisseur bars or eddy currents.

In Fig. 10 the quantities ψ_{qs}, ψ_{ds}, ψ_f are the total instantaneous flux linkages of the q-axis stator, d-axis stator, and field winding, respectively, in the rotor reference frame; ψ_{aq} and ψ_{ad} are the air-gap flux linkages. Similarly, v_{qs}, v_{ds}, e_f, and i_{qs}, i_{ds}, and i_f are the instantaneous q-axis stator, d-axis stator, and field winding voltages and currents, respectively. The torques T_e and T_l are the developed electromagnetic torque and load torque, and ω_r is the rotor speed in equivalent electrical rad/s. The parameters of the machine which appear as potentiometer settings are identified in Table I.

In Fig. 11 the equivalent two-phase d-q voltages and currents in both the stationary and rotating reference frames are developed from the three-phase variables. The superscript 's' has been used in Fig. 11 in order to distinguish the two-phase d-q variables expressed in the stationary reference frame from those referred to the rotor. Also, it can be noted that the zero sequence component has been omitted since the machine is wye-connected. The currents, i_a, i_b, and i_c are the machine line currents while the voltages v_{an}, v_{bn}, and v_{cn} are the motor phase voltages.

Fig. 12 shows the implementation of the current-fed inverter bridge. In the figure the logic-controlled switches on the right-hand side serve to direct the dc link current to one of the three thyristors in the upper half of the bridge and route a return path through one of the three lower-half thyris-

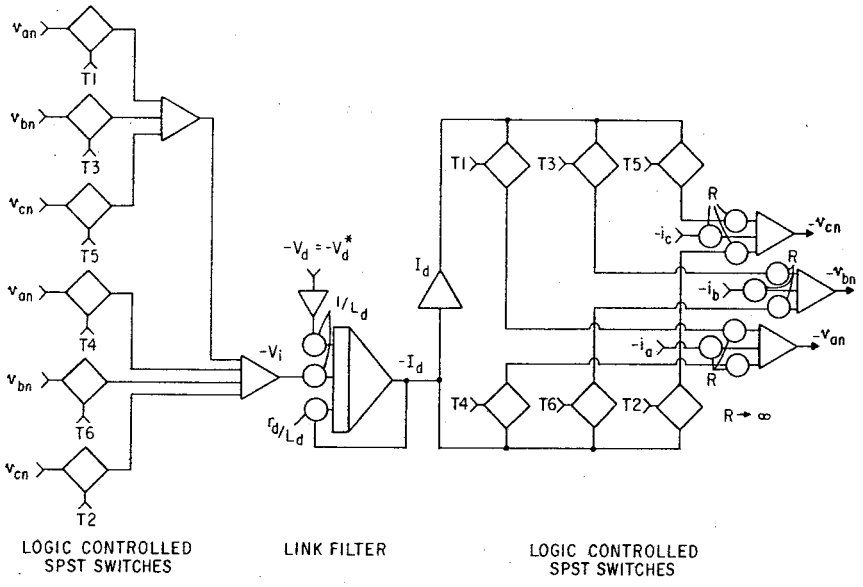

Fig. 12. Simulation of current-fed inverter.

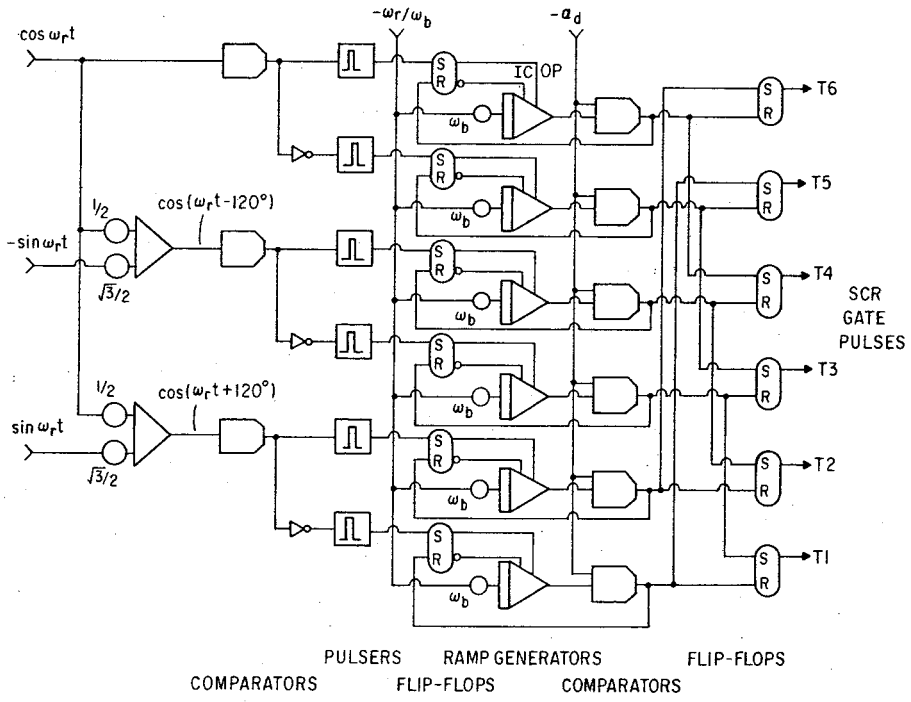

Fig. 13. Simulation of angle control scheme.

tors. The same firing pulses are fed to the left-hand array of switches which function to select the proper voltages corresponding to the two conducting thyristors, summing the result with the proper polarity to make up the dc inverter voltage. The difference between the inverter voltage and the applied dc link voltage V_d is used to compute the dc link current I_d.

It can be observed that the inverter is modeled as an "ideal" current source inverter having negligible commutation time. While it is recognized that commutation effects are more severe in current than in voltage source inverters the time delay due to commutation is predictable and can be readily compensated. If desired, a sampling delay which is a function of link current and air-gap flux (CEMF) can be introduced. Alternatively, more detailed models have been developed which can be used [8]. For purposes of this study, however, such additional accuracy was not deemed necessary. Also, the details of the input ac/dc rectifier are not of interest for this study so that it is assumed that the actual dc link voltage V_d is identically equal to the commanded (desired) value V_d^* derived from the control system.

In Fig. 13 the 120° logic pulses used to drive the inverter are developed. Proceeding from left to right, it can be noted that a three-phase set of sinusoids are developed from the

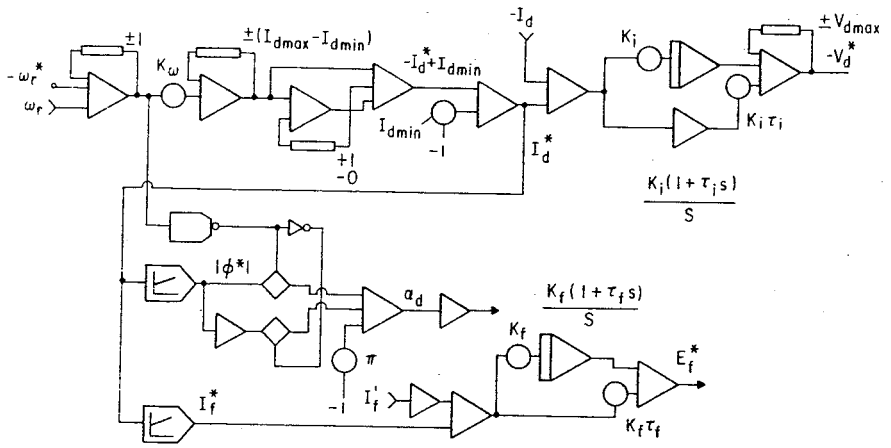

Fig. 14. Simulation of unity displacement factor control system.

variable frequency oscillator which is also used for the voltage and current transformations needed for the simulation of Park's equations. The zero crossings of the sine waves are detected and six clock pulses are produced per 360 electrical degrees rotation and hence model the position encoded pulses of the optical sensors. These clock pulses are used to initiate timed ramps having a slope proportional to rotor speed. The ramp is terminated when the amplitude of the ramp reaches α_d. The outputs of the six right-hand comparators are then interconnected through flip-flops so as to ensure nonoverlapping gate pulses. The signals $T_1, \cdots, T_6$ are 120° gate pulses which are used to trigger the inverter thyristors (SPST switches in the simulation).

The unity displacement factor control system is implemented in Fig. 14. In all cases the asterisk denotes the desired (commanded) value of the variable. It can be noted that two function generators are used to develop the functions ϕ^* versus I_a^* and I_f^* versus I_a^* corresponding to (10), (17), and (18). The desired values of I_d and I_f are regulated by means of the dc link voltage V_d and field voltage E_f. The desired torque angle δ is obtained as shown by the use of the delay angle α_d which is used as the bias signal for the ramp generators in Fig. 13.

Typical computer simulation results are illustrated in Figs. 15 and 16 using the parameters given in Table I. Fig. 15 shows the steady-state waveforms of system variables at 394 Hz, corresponding to a maximum surface (peripheral) speed of 200 mi/h for the prototype linear motor. The machine is operating near rated load (0.85 pu). The computer traces clearly show the "notches" in the machine voltages typical of operation from a current source inverter. In Fig. 16 the machine is subjected to a step increase from an unloaded condition to the same load condition as Fig. 15. It can be noted that the machine responds smoothly to the transient with no tendency towards oscillation or hunting. Similar type of behavior was observed over the entire range of operation from 50 to 394 Hz.

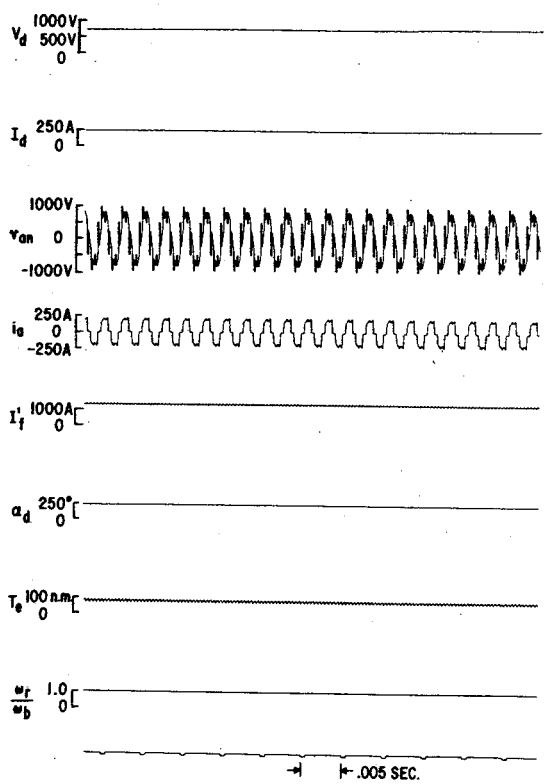

Fig. 15. Simulation of steady-state waveform at rated torque (79.1 N·m) and rated speed (1526 r/min).

VII. DESIGN AND EXPERIMENTATION

The complete control system including the position sensing circuit was designed and tested in the laboratory with the prototype 112-kW inductor machine. A photograph of the machine is shown in Fig. 17 which shows sector wound stator with the field coil at the bottom and the rotor light interrupting studs on the right. The module consisting of optical sensors and associated electronics is located on the shaft supporting bracket. A dc separately excited load machine is coupled to the same shaft for test purpose. The rectifier and inverter of the inductor machine and the load machine with its converters are a part of the general purpose laboratory facility.

In the design of control circuits, the angle and field function generators were approximated by straight lines for simplicity. The digital angle controller was designed to provide 0.33° resolution of SCR firing angle and no appreciable un-

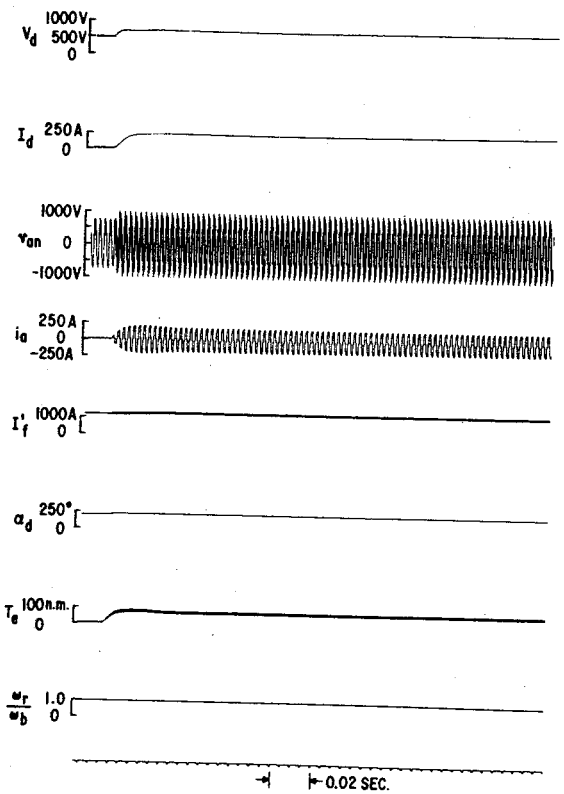

Fig. 16. Simulation response for step increase in load torque from no load to 79.1 N·m 394 Hz.

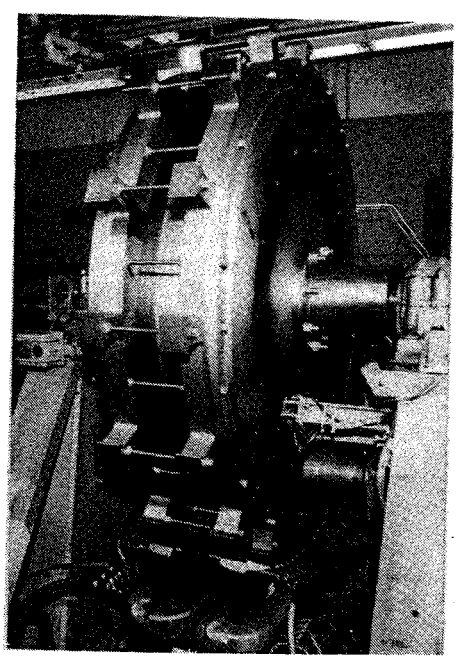

Fig. 17. Experimental 112-kW inductor machine in the laboratory showing position sensing assembly.

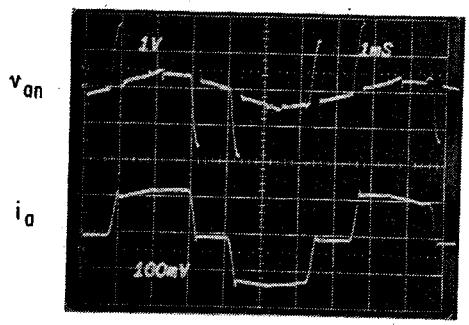

Fig. 18. Scope trace of phase voltage and current at 150 Hz with 200-A dc link current. Vertical scale: 100 V/cm 200 A/cm, respectively. Horizontal scale: 1 ms/cm.

balance was noticed. The overlap angle compensation was fine tuned until desired operation was obtained.

The inductor machine was tested for static and dynamic performance in wide speed and torque ranges and the experimental results agree well with the theory and simulation results. The displacement factor was found to vary between 0.95 and unity because of cumulative effect of several imperfect conditions. Fig. 18 shows the typical phase voltage and current waves at the machine terminal in motoring condition. The current commutation effect and the resulting voltage transient is evident from the figure. Fig. 19 shows the transient response of the machine at constant command speed when step load torque is applied and subsequently removed. This trace can be compared qualitatively to Fig. 16. Note again the well-damped response similar to Fig. 16.

Fig. 20 shows the transient response for step changes in speed command under a constant load torque condition. Note that the armature current responds almost immediately to the sudden error in speed command. Response to a step decrease in speed command is similar, however, in this case a speed decrease is accomplished by regenerative braking. Note that when the rotor speed approaches the desired operating speed the machine automatically switches over to motoring operation. The transition point between braking and motoring is clearly apparent.

VIII. CONCLUSION

A control strategy for a self-controlled sector wound linear inductor machine has been described which permits operation at constant air-gap flux and unity displacement factor under all operation conditions. The machine is capable of motoring and regeneration in wide speed and torque ranges and well balanced firing pulses with 0.33° resolution is obtained through a digital angle controller. The control incorporates an overlap angle compensation scheme which helps to restore unity displacement factor.

The *d-q* axis dynamic model of the machine with the control and converter circuits has been simulated on a hybrid computer and performances have been studied in detail. The control circuit with the position sensors have been designed and tested in the laboratory with a newly designed 112-kW machine, and the experimental results show good agreement with the theory and simulation results.

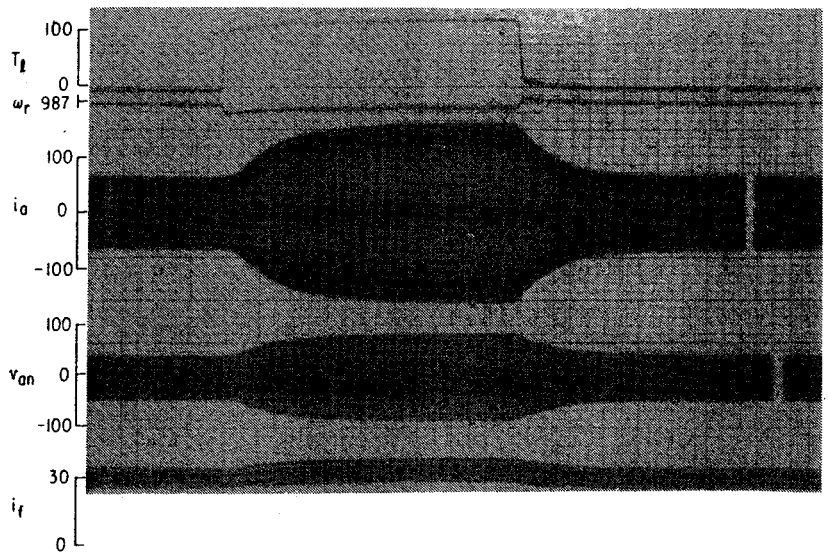

Fig. 19. Transient response with step changes in load torque near 0.4 per unit speed. Speed before application of load: 609 r/min; after: 596 r/min.

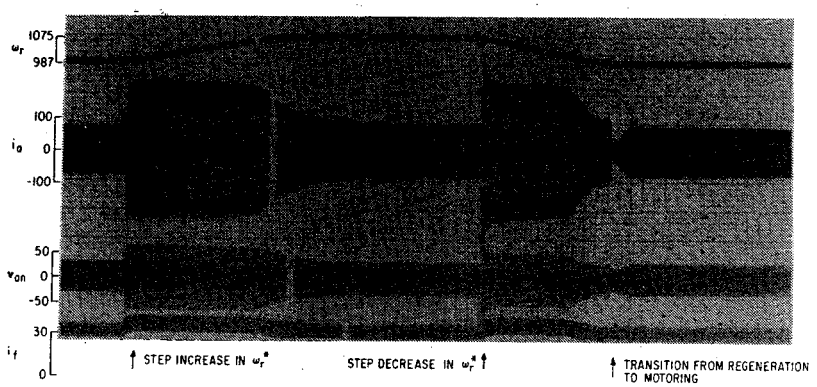

Fig. 20. Transient response with step changes of speed command near 0.4 per unit speed.

ACKNOWLEDGMENT

The authors gratefully acknowledge the help of W. Mischler during the experimental part of the project. Thanks are also due to M. Guarino of DOT-FRA who has guided the exploratory development of the inductor motor.

REFERENCES

[1] A. Häbock and D. Köllensperger, "State of development of converter-fed synchronous motors with self control," *Siemens Rev.*, XXXVIII, pp. 390–392, 1971.

[2] E. Levi, "Linear synchronous motors for high-speed ground transport," *IEEE Trans. Magn.*, vol. MAG-9, pp. 242–248, Sept. 1973.

[3] H. Stemmler, "Drive systems and electronic control equipment of the gearless tube mill," *Brown Boveri Rev.*, vol. 57, pp. 120–128, Mar. 1970.

[4] C. B. Mayer and T. A. Lipo, "Use of simulation in the design of an inverter drive," in *Conf. Rec., 1972 IEEE Ann. Meeting*, pp. 745–752.

[5] B.-T. Ooi, "Homopolar linear synchronous motor dynamic equivalents," *IEEE Trans. Magn.*, vol. MAG-13, pp. 1424–26, Sept. 1977.

[6] R. H. Park, "Two-reaction theory of synchronous machinery, I—Generalized method of analysis, *Trans. AIEE*, vol. 48, pp. 716–730, Jul. 1929.

[7] P. C. Krause and K. Carlsen, "Analysis of a homopolar inductor-alternator," in *Conf. Rec. IEEE Ind. Gen. Appl. Ann. Meeting*, pp. 117–125, 1968.

[8] T.A. Lipo, "Simulation of a current source inverter drive," *Conf. Rec. 1977 PESC Conf.*, pp. 310–315.

Bimal K. Bose (S'59–M'60–SM'78) received the B.E. degree from Calcutta University, Calcutta, India, in 1956, the M.S. degree from University of Wisconsin, Madison, in 1960 and the Ph.D. degree from Calcutta University in 1966.

From 1956 to 1958, he was an Electrical Engineer in Tata Power Co., Bombay, India. In 1960, he joined Bengal Engineering College (Calcutta University) where he organized the Industrial Electronics Program and did research in the areas of magnetic amplifiers, instrumentation, and power electronics. He was awarded the Premchand Roychand Scholarship in 1968 and Mouat Gold Medal in 1970 by Calcutta University for research contributions. In 1971, he joined Rensselaer Polytechnic Institute, Troy, NY, where he was responsible for organizing the power electronics program for six years. He was consultant with several industries which included the General Electric Company and Bendix Corporation. In 1976, he joined General Electric Corporate Research and Development, Schenectady, NY. Currently his research interests are in power electronics, machine control which include microprocessor application to power conversion systems. He has published a number of research papers and holds three patents. At present, he is Adjunct Professor in Rensselaer Polytechnic Institute and Chairman of TRANSACTIONS Review, Static Power Converter Committee, IEEE. Currently he is editing an IEEE book on adjustable speed ac drive systems.

Thomas A. Lipo (M'64–SM'72) for a photograph and biography please see page 24 of the January/February 1979 issue of this TRANSACTIONS.